



## Article

# Anti-Inflammatory, Antiallergic, and COVID-19 Main Protease (M<sup>PRO</sup>) Inhibitory Activities of Butenolides from a Marine-Derived Fungus *Aspergillus terreus*

Ibrahim Seyda Uras<sup>1,2,†</sup>, Sherif S. Ebada<sup>3,4,\*,†</sup> , Michal Korinek<sup>5,6,7,8</sup> , Amgad Albohy<sup>9</sup> ,  
 Basma S. Abdulrazik<sup>9</sup>, Yi-Hsuan Wang<sup>7</sup>, Bing-Hung Chen<sup>6,10,11</sup> , Jim-Tong Horng<sup>12</sup>, Wenhan Lin<sup>13,\*</sup> ,  
 Tsong-Long Hwang<sup>7,8,14,15,\*</sup>  and Belma Konuklugil<sup>1,16,\*</sup>

- 1 Department of Pharmacognosy, Faculty of Pharmacy, Ankara University, Ankara 06560, Turkey; isuras@ankara.edu.tr
  - 2 Department of Pharmacognosy, Faculty of Pharmacy, Agri Ibrahim Cecen University, Agri 04100, Turkey
  - 3 Department of Pharmacognosy, Faculty of Pharmacy, Ain Shams University, Abbasia, Cairo 11566, Egypt
  - 4 Department of Pharmacognosy, Faculty of Pharmacy, Sinai University, Kantara, Ismailia 41511, Egypt
  - 5 Graduate Institute of Natural Products, College of Pharmacy, Kaohsiung Medical University, Kaohsiung 80708, Taiwan; mickorinek@hotmail.com
  - 6 Department of Biotechnology, College of Life Science, Kaohsiung Medical University, Kaohsiung 80708, Taiwan; bhchen@kmu.edu.tw
  - 7 Graduate Institute of Natural Products, College of Medicine, Chang Gung University, Taoyuan 33302, Taiwan; d0901501@cgu.edu.tw
  - 8 Research Center for Chinese Herbal Medicine, Research Center for Food and Cosmetic Safety, and Graduate Institute of Health Industry Technology, College of Human Ecology, Chang Gung University of Science and Technology, Taoyuan 33302, Taiwan
  - 9 Department of Pharmaceutical Chemistry, Faculty of Pharmacy, The British University in Egypt (BUE), El-Sherouk City, Suez Desert Road, Cairo 11837, Egypt; amgad.albohy@bue.edu.eg (A.A.); basma.sabry@bue.edu.eg (B.S.A.)
  - 10 Department of Medical Research, Kaohsiung Medical University Hospital, Kaohsiung 80708, Taiwan
  - 11 The Institute of Biomedical Sciences, National Sun Yat-sen University, Kaohsiung 80424, Taiwan
  - 12 Department of Biochemistry and Molecular Biology, College of Medicine, Chang Gung University, Taoyuan 33302, Taiwan; jimtong@mail.cgu.edu.tw
  - 13 State Key Laboratory of Natural and Biomimetic Drugs, Peking University, Beijing 100083, China
  - 14 Department of Anesthesiology, Chang Gung Memorial Hospital, Taoyuan 33302, Taiwan
  - 15 Department of Chemical Engineering, Ming Chi University of Technology, New Taipei City 24301, Taiwan
  - 16 Department of Pharmacognosy, Faculty of Pharmacy, Lokman Hekim University, Çankaya, Ankara 06510, Turkey
- \* Correspondence: sherif\_elsayed@pharma.asu.edu.eg (S.S.E.); whlin@bjmu.edu.cn (W.L.); htl@mail.cgu.edu.tw (T.-L.H.); konuklugil@pharmacy.ankara.edu.tr (B.K.); Tel.: +20-2405-1180 (S.S.E.); Fax: +20-2405-1107 (S.S.E.)
- † These authors equally contributed to this work.



**Citation:** Uras, I.S.; Ebada, S.S.; Korinek, M.; Albohy, A.; Abdulrazik, B.S.; Wang, Y.-H.; Chen, B.-H.; Horng, J.-T.; Lin, W.; Hwang, T.-L.; et al. Anti-Inflammatory, Antiallergic, and COVID-19 Main Protease (M<sup>PRO</sup>) Inhibitory Activities of Butenolides from a Marine-Derived Fungus *Aspergillus terreus*. *Molecules* **2021**, *26*, 3354. <https://doi.org/10.3390/molecules26113354>

Academic Editor: Enrique Barrajon

Received: 14 May 2021

Accepted: 28 May 2021

Published: 2 June 2021

**Publisher's Note:** MDPI stays neutral with regard to jurisdictional claims in published maps and institutional affiliations.



**Copyright:** © 2021 by the authors. Licensee MDPI, Basel, Switzerland. This article is an open access article distributed under the terms and conditions of the Creative Commons Attribution (CC BY) license (<https://creativecommons.org/licenses/by/4.0/>).

**Abstract:** In December 2020, the U.K. authorities reported to the World Health Organization (WHO) that a new COVID-19 variant, considered to be a variant under investigation from December 2020 (VUI-202012/01), was identified through viral genomic sequencing. Although several other mutants were previously reported, VUI-202012/01 proved to be about 70% more transmissible. Hence, the usefulness and effectiveness of the newly U.S. Food and Drug Administration (FDA)-approved COVID-19 vaccines against these new variants are doubtfully questioned. As a result of these unexpected mutants from COVID-19 and due to lack of time, much research interest is directed toward assessing secondary metabolites as potential candidates for developing lead pharmaceuticals. In this study, a marine-derived fungus *Aspergillus terreus* was investigated, affording two butenolide derivatives, butyrolactones I (1) and III (2), a meroterpenoid, terretonin (3), and 4-hydroxy-3-(3-methylbut-2-enyl)benzaldehyde (4). Chemical structures were unambiguously determined based on mass spectrometry and extensive 1D/2D NMR analyses experiments. Compounds (1–4) were assessed for their in vitro anti-inflammatory, antiallergic, and in silico COVID-19 main protease (M<sup>PRO</sup>) and elastase inhibitory activities. Among the tested compounds, only 1 revealed significant activities comparable to or even more potent than respective standard drugs, which makes butyrolactone I (1)

a potential lead entity for developing a new remedy to treat and/or control the currently devastating and deadly effects of COVID-19 pandemic and elastase-related inflammatory complications.

**Keywords:** *Aspergillus terreus*; butenolides; antiallergic; COVID-19 M<sup>Pro</sup>; elastase

## 1. Introduction

For more than a year now, since 2019, the whole world has been faced with the Coronavirus Disease 2019 (COVID-19) pandemic, believed to be caused by severe acute respiratory syndrome coronavirus 2 (SARS-CoV 2), a zoonotic viral infection that first emerged and was reported in Wuhan, China in December 2019 [1,2]. During this year, scientists from all around the globe set new horizons for collaborations to race against time to produce a dependable and a reliable vaccine. This mission was accomplished in December 2020 when the U.S. Food and Drug Administration (FDA) issued the first Emergency Use Authorization (EUA) for the Pfizer–BioNTech vaccine [3] and the United Kingdom approved the emergency use of the Oxford–AstraZeneca vaccine for the prevention of the COVID-19 in individuals 16 years of age or older [4]. However, simultaneously, two new viral variants were identified at two widely spaced localities in London, United Kingdom, designated as a variant under investigation of December 2020 (VUI-202012/01) and in Cape Town, South Africa, named 501.V2, that both shared a common worrying feature of being up to 70% more transmissible [5]. New variants are not the only ones evolved by SARS-CoV-2, but they are the ones that succeeded in adopting uncontrolled transmission among humans, forcing several countries to move back to strict lockdowns, social distancing and other infection control measures [5]. These two new variants also raised questions about the efficacy and effectiveness of the approved vaccines against them, which will take more time to figure out.

In other domains, more research efforts have been directed toward finding out other treatment alternatives to ease COVID-19 severity in vulnerable patients, especially acute respiratory distress symptoms mainly caused by neutrophil elastase (NE) enzyme, an intracellular enzyme stored in azurophilic granules of polymorphonuclear neutrophils (PMNs) that are a major component of human innate immunity [6,7]. Although NE's main function is to devastate functional proteins of xenobiotics and/or pathogens of various origins, it has also been found to induce deleterious effects on the lungs as elastin-rich connective tissue affording pathologic edematous symptoms such as acute lung injury (ALI), acute respiratory distress syndrome (ARDS), or chronic obstructive pulmonary disorder (COPD) [7,8]. Moreover, NE contributes to the invasion of SARS-CoV-2 into host cells and plays a role in the COVID-associated ARDS, developed usually in the late stage of the COVID disease. Currently, sivelestat is the only approved NE inhibitor for the treatment of ARDS (in Korea and Japan) [9].

Fungi from various environments proved to be a prolific source producing a plethora of secondary metabolites with intriguing spectrum of biological activities and/or industrial applications [10]. The *Aspergillus* genus is among the most abundant fungal genera, comprising about 250 species, and is a major source contributing to the discovery of bioactive fungal metabolites [11]. *Aspergillus terreus* is a widely distributed fungus in diverse environments including extreme living conditions of high salinity [12], high temperature [13], high alkalinity [14], and drought [15]. Its ability to accommodate these extreme conditions stressed its probable evolution of gene clusters or regulatory mechanism to acclimatize these environments that may also induce the biosynthesis of a wide variety of fungal secondary metabolites including alkaloids, polyketides, peptides, terpenes, and lignans [11,16–19]. Butenolides (a rare type of lignans) and terretinins (meroterpenoids) are considered as typical metabolites of the genus *Aspergillus* that have exhibited a wide range of bioactivities such as antibacterial [20], cytotoxic [21], anti-inflammatory [22], antioxidant [23], and antiviral activities [24].

As part of our ongoing research directed toward exploring secondary metabolites for their relevant bioactivities, we investigated those obtained from a marine-derived fungus *Aspergillus terreus* for their *in vitro* anti-inflammatory, antiallergic, and *in silico* molecular modeling against the COVID-19 main protease (M<sup>Pro</sup>) as a potential target for developing an antiviral drug. In this study, we report the isolation and identification of four different fungal metabolites (1–4) (Figure 1), their *in vitro* bioactivity assessment, and their *in silico* docking study results.

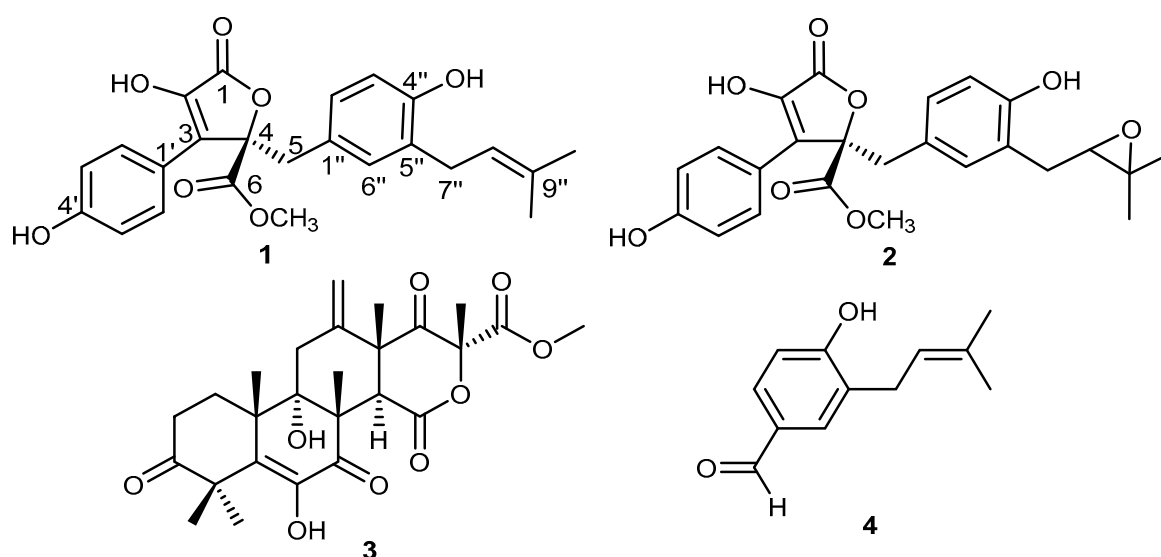


Figure 1. Chemical structures of 1–4.

## 2. Results and Discussion

### 2.1. Isolation and Characterization of Main Secondary Metabolites in the Fungal Extract

A detailed chromatographic investigation of the solid rice culture extract from the cultivated fungal strain *Aspergillus terreus* derived from the marine annelide *Spirorbis* sp. was performed by applying different chromatographic procedures; that is, MS, 1D and 2D NMR spectral analyses, and comparing the obtained results with the reported literature. The obtained results afforded four different compounds.

Compound 1 was isolated as an orange-coloured amorphous solid. Its UV spectrum revealed two absorption maxima ( $\lambda_{\max}$ ) at 210 and 307 nm. The HRESIMS revealed the presence of two pseudomolecular ion peaks at  $m/z$  447.12980 [ $M + Na$ ]<sup>+</sup> (calcd. for C<sub>24</sub>H<sub>24</sub>O<sub>7</sub>Na, 447.13092) and at  $m/z$  423.12077 [ $M - H$ ]<sup>−</sup> (calcd. for C<sub>24</sub>H<sub>23</sub>O<sub>7</sub>, 423.12201). Hence, the molecular formula was established to be C<sub>24</sub>H<sub>24</sub>O<sub>7</sub>, indicating the existence of 13 degrees of unsaturation. The <sup>13</sup>C NMR, DEPT, and HMQC spectra of 1 differentiated the presence of 11 quaternary carbons including two carbonyl groups ( $\delta_C$  170.1 and  $\delta_C$  169.8), three oxygenated olefinic carbons ( $\delta_C$  157.2,  $\delta_C$  153.2, and  $\delta_C$  144.9), five olefinic carbons ( $\delta_C$  137.7, 133.9, 128.8, 124.6, and 121.8), and one aliphatic quaternary carbon ( $\delta_C$  86.2). In addition, eight tertiary, two secondary, and three primary carbons were also distinguished. The <sup>1</sup>H NMR spectrum of 1 clearly revealed the existence of two different aromatic systems, one recognized as 1,4-disubstituted phenyl and illustrated by two proton resonances each integrated for two protons at  $\delta_H$  6.90 (2H, d,  $J$  = 8.8 Hz) and at  $\delta_H$  7.61 (2H, d,  $J$  = 8.8 Hz). The second aromatic spin system was shown to be an 1,3,4-trisubstituted aromatic moiety as represented by three different proton resonances at  $\delta_H$  6.59 (1H, dd,  $J$  = 8.1, 2.0 Hz),  $\delta_H$  6.52 (1H, d,  $J$  = 8.1 Hz), and  $\delta_H$  6.51 (1H, d,  $J$  = 2.0 Hz). Moreover, the <sup>1</sup>H NMR spectrum displayed three singlet methyl groups including one oxygenated methoxy group ( $\delta_H$  3.75/ $\delta_C$  53.7) and two olefinic methyl groups at  $\delta_H$  1.65 and  $\delta_H$  1.59 ppm directly connected to carbon peaks at  $\delta_C$  25.7 and  $\delta_C$  17.7 ppm, respectively. By comparing the obtained data with the reported fungal metabolites in the literature, they revealed a great

agreement to butyrolactone I, a butenolide fungal metabolite first reported from *Aspergillus terreus* var. *Africans* IFO8355 [25–27].

Compound **2** was purified as a yellow-coloured amorphous solid showing absorption maxima ( $\lambda_{\max}$ ) in its UV spectrum at 225 and 308 nm similar to those shown by **1**. The HRESIMS of **2** exhibited two pseudomolecular ion peaks at  $m/z$  463.12586  $[M + Na]^+$  (calcd. for  $C_{24}H_{24}O_8Na$ , 463.12691) and at  $m/z$  439.11538  $[M - H]^-$  (calcd. for  $C_{24}H_{23}O_8$ , 439.11654), indicating the molecular formula to be  $C_{24}H_{24}O_8$ , differing by an additional oxygen atom compared with butyrolactone I (**1**) and similarly having 13 degrees of unsaturation. The  $^1H$  and  $^{13}C$  NMR spectra of **2** revealed a close similarity to **1**, except for the disappearance of the characteristic isoprenyl peaks and the existence of two oxygenated  $sp^3$  carbons differentiated into one methine ( $\delta_C$  69.7) and one aliphatic quaternary carbon ( $\delta_C$  76.8) together with two singlet methyl groups at  $\delta_H$  1.21 ( $\delta_C$  24.8) and  $\delta_H$  1.24 ( $\delta_C$  22.0). The HMBC spectrum of **2** exhibited clear long-range correlations from the two singlet methyl groups to two carbons at  $\delta_C$  69.7 and  $\delta_C$  76.8, suggesting the replacement of isoprenyl moiety by an epoxy ring. By searching the reported literature, compound **2** was confirmed to be butyrolactone III [28,29].

Compound **3** was obtained as a creamy-coloured amorphous solid, with its UV spectrum showing two absorption maxima ( $\lambda_{\max}$ ) at 220 and 278 nm. The molecular formula was determined to be  $C_{26}H_{32}O_9$  based on its HRESIMS spectrum, which disclosed the presence of two pseudomolecular ion peaks at  $m/z$  489.2070  $[M + H]^+$  (calcd. for  $C_{26}H_{33}O_9$ , 489.2125), at  $m/z$  511.1887  $[M + Na]^+$  (calcd. for  $C_{26}H_{32}O_9Na$ , 511.1944), and at  $m/z$  487.1971  $[M - H]^-$  (calcd. for  $C_{26}H_{31}O_9$ , 487.1968), indicating the existence of 11 degrees of unsaturation. Both 1D and 2D NMR spectra of **3** revealed a similar pattern to those presented by terretonin, a meroterpenoid previously reported from *A. terreus* fungus [30,31].

Compound **4** was obtained as a red-coloured solid powder. Its  $^{13}C$  NMR spectrum revealed twelve distinct carbon resonances that can be differentiated through  $^1H$  NMR and HMQC experiment into four quaternary ( $\delta_C$  161.1, 132.2, 128.5, and 128.4), five tertiary including one aldehyde carbon at  $\delta_C$  191.1 s, together with three aromatic carbons ( $\delta_C$  130.7,  $\delta_C$  130.1, and  $\delta_C$  115.1) and an olefinic carbon at  $\delta_C$  121.9 [ $\delta_H$  5.29 (1H, td,  $J = 7.4$ , 1.5 Hz)]; one secondary carbon at  $\delta_C$  27.7 [ $\delta_H$  3.26 (2H, d,  $J = 7.4$  Hz)]; in addition to two primary carbons at  $\delta_C$  25.5 [ $\delta_H$  1.71 (3H, d,  $J = 1.5$  Hz)], and  $\delta_C$  17.6 [ $\delta_H$  1.68 (3H, d,  $J = 1.5$  Hz)]. The  $^1H$  NMR spectrum in DMSO- $d_6$  revealed a clear 1,3,4-trisubstituted aromatic moiety through three proton resonances at  $\delta_H$  7.60 (1H, d,  $J = 8.2$ , 2.2 Hz),  $\delta_H$  7.58 (1H, d,  $J = 2.2$  Hz), and  $\delta_H$  6.95 (1H, d,  $J = 8.2$  Hz). In addition, it also showed two deshielded protons at  $\delta_H$  10.58 and  $\delta_H$  9.75 ppm ascribed for an aromatic hydroxyl group and an aldehyde moiety, respectively. By comparing the obtained 1D and 2D NMR data of **4** with the reported literature, it turned out to be identical to those reported for 4-hydroxy-3-(3-methylbut-2-enyl)benzaldehyde, a fungal metabolite first reported in 2012 from the root rotting pathogen *Heterobasidion occidentale* [32] and later reported from the fruits of *Narthecium ossifragum* [33].

Based on the previous reports about the activity of butyrolactones, they have been distinguished as potent inhibitors of cyclin-dependent kinases (CDKs) that play an important role in the occurrence of various diseases such as cancer, Alzheimer's disease, Parkinson's disease, stroke, diabetes, glomerulonephritis, and inflammation. Isolated butyrolactones (**1** and **2**) along with terretonin (**3**) and 4-hydroxy-3-(3-methylbut-2-enyl)benzaldehyde (**4**) were subjected to in vitro antiallergic, anti-inflammatory, anti-HCoV-229, and neutrophil elastase enzymatic assays. The viability assays towards the cells used in the tests were also performed.

## 2.2. Degranulation Assay in Mast Cells

The toxicity of isolated compounds was tested on RBL-2H3 cells up to 100  $\mu$ M. The results revealed that all tested compounds were non-toxic as illustrated by the viability rate exceeding 90%. Isolated compounds (**1–4**) were then tested for their antiallergic

activity via determining their inhibitory activities against A23187- and antigen-induced  $\beta$ -hexosaminidase release in RBL-2H3 cells. Calcium ionophore A23187 induces calcium transport into the mast cell membrane, whereas antigen (IgE plus DNP-BSA) acts via the Fc $\epsilon$ RI receptor, resembling a physiological condition. The attained results (Table 1) displayed that only butyrolactone I (1), among the tested compounds, showed moderate antiallergic activity, illustrated via inhibiting A23187- and antigen-induced degranulation with IC<sub>50</sub> values of 39.7 and 41.6  $\mu$ M, respectively, compared with azelastine as a standard antiallergic drug (34.5 and 35.5% at 10  $\mu$ M, respectively). The obtained results are in accordance with and supported by the previously reported activity of 1 in alleviating ovalbumin-induced allergy symptoms via reducing the levels of histamine and mouse mast cell proteinases [34].

**Table 1.** Inhibitory activity of butyrolactone I (1) on A23187- and antigen-induced degranulation.

Compound.	Cell Viability, RBL-2H3 <sup>a</sup>	Inhibition of A23187-Induced Degranulation <sup>b</sup>	Inhibition of Antigen-Induced Degranulation <sup>c</sup>
	% (100 $\mu$ M)	IC <sub>50</sub> ( $\mu$ M) <sup>d</sup>	IC <sub>50</sub> ( $\mu$ M) <sup>d</sup>
Butyrolactone I (1)	>90%	39.7 <sup>e</sup>	41.6 <sup>f</sup>
Butyrolactone III (2)	>90%	>100	>100
Terretonin (3)	>90%	>100	>100
4-Hydroxy-3-(3-methylbut-2- enyl)benzaldehyde (4)	>90%	>100	>100

<sup>a</sup> The cytotoxicity of samples to RBL-2H3 was evaluated using MTT viability assay. The results are presented as mean ( $n = 3$ ) compared with untreated control (DMSO). All samples were nontoxic towards RBL-2H3 cells. <sup>b</sup> Azelastine (10  $\mu$ M) was used as a positive control and inhibited  $34.5 \pm 2.5\%$  of A23187-induced degranulation. The inhibition of degranulation was assessed by A23187-induced  $\beta$ -hexosaminidase release in RBL-2H3 cells. The results are presented as mean  $\pm$  S.E.M. ( $n = 3$ ). <sup>c</sup> Azelastine (10  $\mu$ M) was used as a positive control and inhibited  $35.5 \pm 8.1\%$  of antigen-induced degranulation. The inhibition of degranulation was assessed by antigen-induced  $\beta$ -hexosaminidase release in RBL-2H3 cells. The results are presented as mean  $\pm$  S.E.M. ( $n = 3$ ). <sup>d</sup> Concentration necessary for 50% inhibition (IC<sub>50</sub>). <sup>e</sup> Butyrolactone I (1) showed dose-dependent inhibition of A23187-induced degranulation with  $26.0 \pm 2.4\%$  (10  $\mu$ M) and  $98.7 \pm 0.7\%$  inhibition at 100  $\mu$ M. <sup>f</sup> Butyrolactone I (1) showed dose-dependent inhibition of antigen-induced degranulation with  $30.0 \pm 3.3\%$  (10  $\mu$ M) and  $87.0 \pm 2.4\%$  inhibition at 100  $\mu$ M. >100, not active (insignificant inhibition of degranulation at 100  $\mu$ M, below 20%).

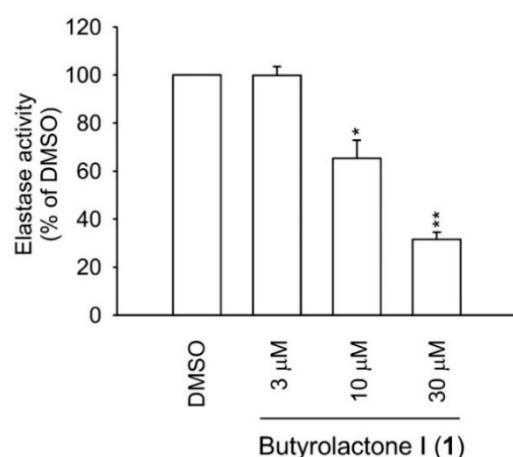
### 2.3. Human Neutrophil Viability, Elastase Release, and Elastase Enzymatic Assays

The results of an in vitro anti-inflammatory assay of compounds 1–4 (Table 2) revealed that only butyrolactone I (1) featured potent inhibitory activities against neutrophil elastase release (IC<sub>50</sub> = 2.30  $\mu$ M). Interestingly, butyrolactone I (1) rather than III (2) exhibited significant activities more potent than genistein used as a standard drug (IC<sub>50</sub> = 32.67  $\mu$ M). Further, the cell viability assay based on lactate dehydrogenase release was performed to exclude toxic effects of 1 on human neutrophils. Both butyrolactone I (1) and III (2) were non-toxic to neutrophils (Table 2). Human neutrophil elastase plays a pivotal role in the development of several inflammatory symptoms including respiratory harmful effects accompanying several acute and chronic respiratory disorders [8]. In the cell-free system, butyrolactone I (1) revealed a dose-dependent direct inhibitory effect on the enzymatic activity of elastase (Figure 2) with an IC<sub>50</sub> value of 16.70  $\mu$ M (Table 2). Based on these results, the anti-inflammatory effects of 1 were, at least partly, attributed to its interaction with elastase enzyme. Therefore, we performed the following in silico molecular modeling experiment to simulate and identify the interaction sites.

**Table 2.** Effects of the isolated compounds from the marine-derived fungus *Aspergillus terreus* on elastase release, viability, and elastase enzymatic activity in vitro.

Compound	Elastase Release in Human Neutrophils <sup>a</sup>	Cell viability, Human Neutrophils <sup>c</sup>	Elastase Enzymatic Activity (Cell-Free) <sup>d</sup>
	IC <sub>50</sub> (μM) <sup>b</sup>	% (10 μM)	IC <sub>50</sub> (μM) <sup>b</sup>
Butyrolactone I (1)	2.30 ± 0.27	94.13 ± 2.31	16.70 ± 2.64
Butyrolactone III (2)	>10	98.25 ± 1.77	>30
Terretonin (3)	>10	n.t.	n.t.
4-Hydroxy-3-(3-methylbut-2-enyl)benzaldehyde (4)	>10	n.t.	n.t.

<sup>a</sup> Inhibition of elastase release in fMLF/cytochalasin B (CB)-induced human neutrophils. Genistein inhibited elastase release with an IC<sub>50</sub> value 32.67 ± 1.45. <sup>b</sup> Concentration necessary for 50% inhibition (IC<sub>50</sub>). The results are presented as mean ± S.E.M. (n = 3). \* p < 0.05, \*\* p < 0.01, \*\*\* p < 0.001 compared with the control (0.1% DMSO). <sup>c</sup> Percentage of cell viability (%) at 10 μM. The results are based on the lactate dehydrogenase release and presented as mean ± S.E.M. (n = 3). <sup>d</sup> Sivelestat was used as a positive control and inhibited elastase enzyme with an IC<sub>50</sub> value 17.92 ± 4.66 nM. n.t.: not tested.

**Figure 2.** In vitro elastase inhibitory activity of butyrolactone I (1) in the cell-free system. The results are presented as mean ± S.E.M. (n = 3). \* p < 0.05, \*\* p < 0.01 compared with the control (0.1% DMSO).

#### 2.4. Molecular Docking Studies

Docking studies were used to investigate the affinity of isolated compounds to the human neutrophil elastase (NE). The crystal structure of NE is available in the protein data bank (PDB) with the ID 1H1B co-crystallized with GW475151. Validation of the docking procedure was reported earlier, where the co-crystallized ligand was redocked in the active site with a docking score of −6.9 kcal/mol, and an RMSD of 1.317 between docked, and crystallized structures [35]. The co-crystallized ligand is known to form a hydrogen bond with Ser195 that is important for binding [36]. In this study, we have docked the isolated compounds (1–4) in the active site of the human NE. Out of the tested compounds, only butyrolactone I (1) has shown a docking score superior to that of the co-crystallized ligand (Table 3). All of tested compounds were found to form a hydrogen bond with Ser195 similar to GW475151, the co-crystallized ligand. It is worth mentioning here that 1 was found to inhibit human elastase in vitro with an IC<sub>50</sub> of 16.70 μM (Table 2). The binding mode of compound 1 as well as its interaction with amino acids in the active site is shown in Figure 3. Butyrolactone III (2), which is a very similar structure, did not show similar results in either elastase assays (Table 3, no noticed inhibition at concentration up to 10 μM) or docking study. This might be attributed to the fact that the isoprene part of butyrolactone I (1) is docked in a hydrophobic side pocket, forming hydrophobic interactions with Phe21 and Leu99, as can be seen in Figure 3. This binding mode will not be favored for the epoxide ring of butyrolactone III (2), leading to a flipped alternative binding mode that is missing the key interaction with Ser195.

**Table 3.** Docking results of tested compounds in the active sites of human NE (1H1B) and SARS-CoV-2 main protease (6LU7). Amino acids' interactions with both the co-crystallized ligands and tested ligands are shown bold.

Ligand	1H1B (Elastase)		6LU7 (M <sup>Pro</sup> )	
	Binding Affinity (kcal/mol)	Interacting Residues	Binding Affinity (kcal/mol)	Interacting Residues
Butyrolactone I (1)	−7.3	<b>Ser195</b> -Arg147	−7.3	<b>Gly143</b> - <b>Ser144</b> - <b>His163</b> - <b>Glu166</b>
Butyrolactone III (2)	−6.7	<b>Ser195</b> -Arg147	−7.8	Thr26- Leu141- <b>Gly143</b> - <b>Ser144</b> - Cys145- <b>His163</b> - <b>Glu166</b>
Terretonin (3)	−6.7	<b>Ser195</b> - Val216	−7.8	Asn142- <b>Gly143</b> - <b>His163</b>
4-Hydroxy-3-(3-methylbut-2-enyl)benzaldehyde (4)	−5.1	<b>Ser195</b> - Cyc191	−5.6	Leu141- <b>Gly143</b> -Ser144-Cys145- <b>Glu166</b>
1H1B-Ligand	−6.9	<b>Ser195</b>	−	−
6lu7-Ligand	−	−	−7.1 (3rd pose)	Phe140, Gly143, His163, His164, Glu166, Gln189, Thr190

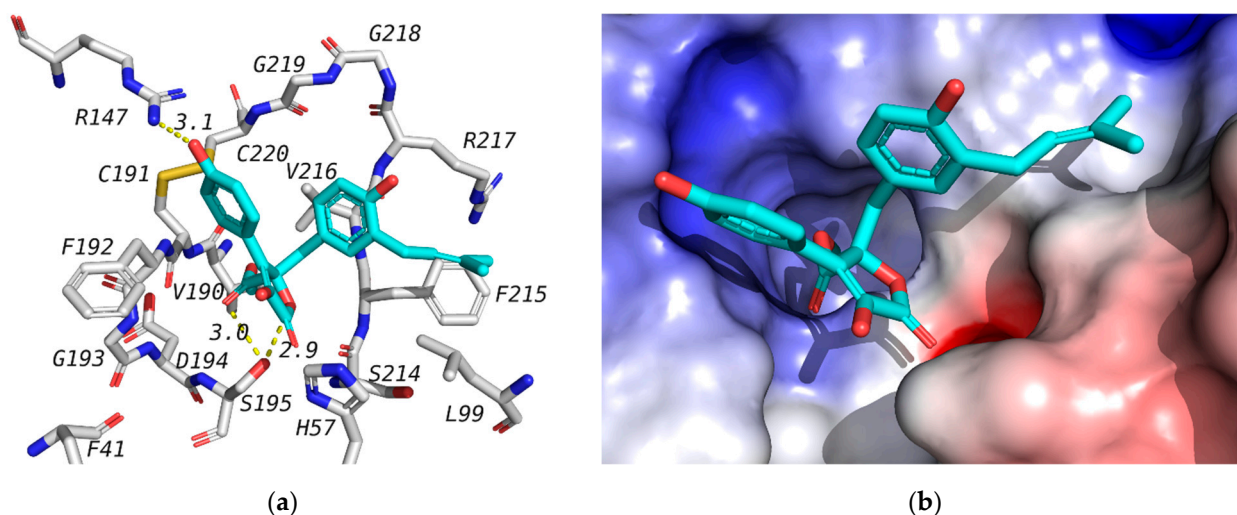


**Figure 3.** Docking of compound butyrolactone I (1) (blue) in the active site of human NE. (a) Interactions of 1 with amino acids in the active site. (b) Docking pose of 1.

In addition to the human NE, we were also interested in investigating the potential binding and inhibitory activities of isolated compounds against SARS-CoV-2 main protease (M<sup>Pro</sup>) owing to the current pandemic situation. The viral main protease is a key enzyme in the virus life cycle that has been the target for several investigations since the beginning of last year. The target crystal structure is available under PDB ID of 6LU7 co-crystallized with a peptide-like inhibitor called N3 [35]. It was found to interact with several amino acids in the active site, including Phe140, Gly143, His163, His164, Glu166, Gln189, and Thr190. Several research groups investigated synthetic and natural products for their inhibition of this target among other SARS-CoV-2 targets [36–38]. We have previously used the same target to investigate the potential inhibition of phytochemicals from the Jordanian hawksbeard [39]. We also reported validation of the same docking procedure through the docking of N3 co-crystallized ligand in the active site of 6LU7 [39]. The docking score of the co-crystallized ligand was found to be −7.1 kcal/mol.

Among the tested compounds, butyrolactone III (2) and terretonin (3) have shown the best scores (−7.8 kcal/mol) compared with the co-crystallized ligand N3 (−7.1 kcal/mol), as shown in Table 3. Both compounds were found to bind in the same pocket where N3 binds, but each overlaps with slightly different parts of N3, as shown in Figure 4. In addition, both compounds were able to maintain two of the hydrogen bonds seen with N3, which include hydrogen bonds with Gly143 and His163.

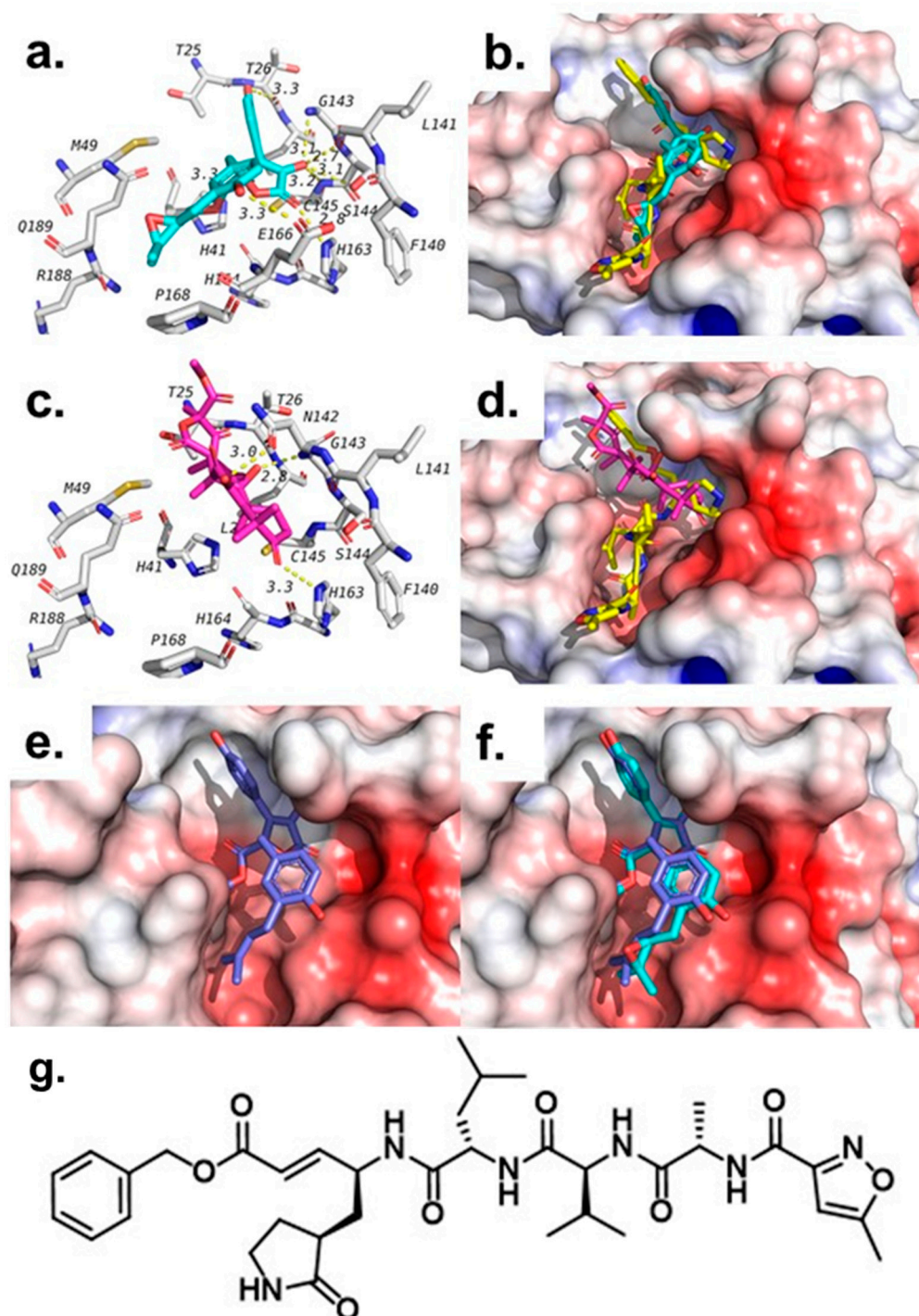


**Figure 4.** Poses and interactions of tested compounds in the active site of SARS-CoV-2 main protease (6LU7). (a) Interactions of butyrolactone III (2) (Cyan) in the active site. (b) Overlapping of butyrolactone III (2) with co-crystallized ligand N3 (yellow). (c) Interactions of terretinin (3) (pink) in the active site. (d) Overlapping of terretinin (3) with co-crystallized ligand N3 (yellow). (e) Binding pose of butyrolactone I (1). (f) Overlapping of the binding poses of butyrolactone I (1) and butyrolactone III (2). (g) Structure of the co-crystallized ligand (N3) in 6LU7 pdb file.

Beside these two hydrogen bonds, both compounds were found to form other hydrogen bonds and hydrophobic interactions with residues in the active site of the SARS-CoV-2 main protease, as shown in Table 3 and Figure 4. In addition to these two compounds, butyrolactone I (1) has also shown a docking score that is better than that of the co-crystallized



ligand (N3), but weaker than 2 and 3. The docking pose of butyrolactone I (1) in the active site of the main protease is shown in Figure 4e. This docking pose is very similar, as expected, to the proposed binding pose of butyrolactone III (2), as seen in Figure 4f. Compound 4, on the other hand, showed the lowest binding affinity (-5.6 kcal/mol) to SARS-CoV-2 main protease compared with the co-crystallized ligand N3. Furthermore, we performed an in vitro human coronavirus 229E (HCoV-229) assay to determine possible protective effects of compounds 1–4 (10  $\mu$ M) against the HCoV-229 infection in Huh7 cells; however, none of the compounds exerted effects (see supplementary materials, Figure S1).

These results suggest a potential role of these isolated compounds in the inhibition of the SARS-CoV-2 main protease with a possible role in controlling the new virus and late stage of coronavirus-associated ARDS inflammation. The results also support the need for further investigation of these compounds as well as the natural products reservoir for new leads that could help us with our battle against the COVID-19 virus.

### 3. Materials and Methods

#### 3.1. General Experimental Procedures

A Perkin-Elmer-241 MC polarimeter was used for determining optical rotation. Chromatographic separation procedures were performed applying column chromatography with different stationary phases such as silica gel 60 M (0.04–0.063 mm) and Sephadex LH20. For screening purposes, ready-made silica gel 60 F<sub>254</sub> TLC plates (Merck, Darmstadt, Germany) were used. For visualization purposes of TLC plates, UV light at 254 and 365 nm wavelengths was applied as a non-destructive technique or after spraying with anisaldehyde reagent and heating. Final purification of fractions was achieved using preparative HPLC (Agilent, Santa Clara, CA, U.S.A.) on Zorbax Eclipse XDB-C18 (Agilent technologies, Santa Clara, CA, U.S.A.) preparative column (9.4 mm  $\times$  250 mm, L  $\times$  ID; 5  $\mu$ m particle size) at a flow rate of 2 mL/min and UV screening detection at 210 to 330 nm. A standard gradient elution was applied using (MeOH, in Water): 0 min, 10% MeOH; 5 min, 10% MeOH; 40 min, 90% MeOH, with a flow rate of 1 mL/min. Each solvent ratio/flow timetable will be present for the compounds purified by HPLC. Preparative TLC separation was done using Flat Bottom TLC Chamber (Camag<sup>®</sup>, Muttenz, Switzerland). Silica gel 60 (0.04–0.063, Merck, Darmstadt, Germany) and Sephadex<sup>®</sup> LH-20 (Sigma-Aldrich, St. Louis, MO, USA) were used for column chromatography and separation was monitored using normal phase silica gel precoated plates F<sub>254</sub> (Merck, Darmstadt, Germany). An Agilent 600 MHz spectrometer (Santa Clara, CA, USA) was used for 1D (<sup>1</sup>H and <sup>13</sup>C NMR) and 2D NMR spectra (chemical shifts in ppm). Chloroform-*d*, DMSO-*d*<sub>6</sub> and methanol-*d*<sub>4</sub> NMR solvents (Sigma Aldrich, Munich, Germany) were used to dissolve the isolated compounds. Supplementary materials of this study includes HPLC chromatograms, Mass, 1D, and 2D NMR spectra of isolated compounds along with NMR data for each compound in a tabulated form.

#### 3.2. Sponge and Fungal Strain Material

The fungus *Aspergillus terreus* was separated from the annelide *Spirorbis* sp., which was collected by one of our co-authors (B.G.) from Marmara Sea, İstanbul, Turkey in July, 2018. For identification, this fungus was cultured on Sabouraud 4% dextrose agar (SDA, Merck, Germany) at room temperature for a week in an incubator (Nüve, Turkey). The fungus was identified as *Aspergillus terreus* (GenBank accession number MT273950) based on DNA amplification and ITS (internal transcribed spacer) sequencing data analysis, as reported previously in the literature. This fungal strain was deposited in the laboratory of the Department of Pharmacognosy, Faculty of Pharmacy, Ankara University (B.K.).

#### 3.3. Fermentation, Extraction, and Isolation

The fungal strain was cultivated on a 100 mL solid rice medium prepared by autoclaving (100 g of rice and 100 mL of distilled water containing 3.5% artificial sea salt

in a 60-piece 2000 mL Erlenmeyer flask). Fermentation continued for 30 days at room temperature away from light under static conditions.

To discontinue the fermentation process, ethyl acetate (EtOAc) ( $3 \times 350$  mL) was added to each flask to stop the growth of cells. After adding EtOAc, flasks were shaken for 12 h, then filtered, and EtOAc filtrate was pooled and evaporated under reduced pressure until yielding a solid residue (3.7 g). The crude extract was then partitioned between *n*-hexane and 90% aqueous MeOH by liquid–liquid fractionation, where both fractions were collected and dried up under vacuum. The aqueous 90% MeOH phase (1.3 g) was subjected to vacuum liquid chromatography (VLC) using silica gel 60 as a stationary phase and the mobile phase started with *n*-hexane/EtOAc (30:70) followed by a gradient elution development of DCM/MeOH (100:0, 90:10, 80:20, 70:30, 60:40, 50:50, 30:70, 10:90, 0:100), respectively, affording ten fractions (AT-1~AT-10).

All obtained fractions were subjected to TLC and analytical HPLC procedures. Fraction AT-2 was chosen for further preparative TLC and HPLC purification procedures. Fraction AT-2 (272 mg), eluted with DCM/MeOH (100:0), was applied on column chromatography using silica gel (Qingdao Haiyang Chemical HG/T2354-92) as stationary phase and petroleum ether/EtOAc as mobile phase at ratios of 4:1, 3:1, 2:1, and 1:1, each 300 mL, respectively, yielding **1** (4.4 mg), **2** (5.3 mg), and **4** (1.8 mg). The subfraction of AT-4 (78 mg) from silica column application was applied on column chromatography using silica gel as the stationary phase and petroleum ether/EtOAc as the mobile phase at ratios of 4:1, 3:1, 2:1, and 1:1, each 200 mL, followed by preparative HPLC for final purification to yield **3** (2.0 mg).

*Butyrolactone I* (**1**). Orange-coloured amorphous solid;  $[\alpha]_D^{20} +91.0^\circ$  (*c* 0.02, MeOH); UV (MeOH)  $\lambda_{\max}$  210 and 307 nm;  $^1\text{H}$  and  $^{13}\text{C}$  NMR, see supplementary material Table S1; HRESIMS  $m/z$  447.12980  $[\text{M} + \text{Na}]^+$  (calcd. for  $\text{C}_{24}\text{H}_{24}\text{O}_7\text{Na}$ , 447.13092) and at  $m/z$  423.12077  $[\text{M} - \text{H}]^-$  (calcd. for  $\text{C}_{24}\text{H}_{23}\text{O}_7$ , 423.12201).

*Butyrolactone III* (**2**). Yellow-coloured amorphous solid;  $[\alpha]_D^{20} +76.0^\circ$  (*c* 0.02, MeOH); UV (MeOH)  $\lambda_{\max}$  225 and 308 nm;  $^1\text{H}$  and  $^{13}\text{C}$  NMR, see supplementary material Table S2; HRESIMS  $m/z$  463.12586  $[\text{M} + \text{Na}]^+$  (calcd. for  $\text{C}_{24}\text{H}_{24}\text{O}_8\text{Na}$ , 463.12691) and at  $m/z$  439.11538  $[\text{M} - \text{H}]^-$  (calcd. for  $\text{C}_{24}\text{H}_{23}\text{O}_8$ , 423.11654).

*Terretonin* (**3**). Creamy-coloured amorphous solid;  $[\alpha]_D^{20} -112.4^\circ$  (*c* 0.02, MeOH); UV (MeOH)  $\lambda_{\max}$  220 and 278 nm;  $^1\text{H}$  and  $^{13}\text{C}$  NMR, see supplementary material Table S3; HRESIMS  $m/z$  489.2070  $[\text{M} + \text{H}]^+$  (calcd. for  $\text{C}_{26}\text{H}_{33}\text{O}_9$ , 489.2125),  $m/z$  511.1887  $[\text{M} + \text{Na}]^+$  (calcd. for  $\text{C}_{26}\text{H}_{32}\text{O}_9\text{Na}$ , 511.1944), and  $m/z$  487.1971  $[\text{M} - \text{H}]^-$  (calcd. for  $\text{C}_{26}\text{H}_{31}\text{O}_9$ , 487.1968).

*4-Hydroxy-3-(3-methylbut-2-enyl)benzaldehyde* (**4**). Red-coloured solid powder;  $^1\text{H}$  and  $^{13}\text{C}$  NMR, see supplementary material Table S4.

### 3.4. Degranulation Assay and MTT Cell Viability Assay in Mast Cells

The mucosal mast-cell-derived rat basophilic leukemia cells (RBL-2H3) were purchased from Bioresource Collection and Research Center (Hsin-Chu, Taiwan). The cells were cultured in DMEM containing 10% FBS, 100 U/mL penicillin, and 100  $\mu\text{g}/\text{mL}$  streptomycin in 10 cm cell culture dishes at  $37^\circ\text{C}$  in a humidified chamber with 5%  $\text{CO}_2$  in air. The level of degranulation in RBL-2H3 cells was evaluated using  $\beta$ -hexosaminidase release assay induced by A23187 or antigen as reported before with some modifications [40]. Briefly, the cells were seeded in a 96-well plate ( $2 \times 10^4$  cells/well, for the A23187-induced assay) or a 48-well plate ( $3 \times 10^4$  cells/well, for the antigen-induced assay) overnight. The cells for the antigen-induced assay were sensitized with anti-DNP IgE (0.5  $\mu\text{g}/\text{mL}$ ; Sigma) during seeding overnight. RBL-2H3 cells were then treated with the samples (0.5, 5, and 50  $\mu\text{M}$ ) for 30 min in Tyrode's buffer with a maximal DMSO dose of 0.5%. For the A23187-induced assay, the cells were activated by addition of A23187 (final concentration 0.5  $\mu\text{M}$ ), while cells for the antigen-induced assay were activated by the addition of DNP-BSA (final

concentration 100 ng/mL) for 30 min. Azelastine (10  $\mu\text{M}$ ) served as the positive control. The amount of  $\beta$ -hexosaminidase was detected using the method utilizing p-NAG as the substrate according to the procedure described before [41].

The viability of the RBL-2H3 cells in the presence of the samples (10 and 100  $\mu\text{M}$ ) was determined using the methylthiazole tetrazolium (MTT) assay according to a previous method [41].

### 3.5. Elastase Release Assay and Lactate Dehydrogenase (LDH) Viability Assay by Human Neutrophils

The human neutrophils were obtained from venous blood of healthy adult volunteers (20–30 years old) following the reported procedure [42]. Elastase release by the activated neutrophils was determined using elastase substrate (*N*-methoxysuccinyl-Ala-Ala-Pro-Val-*p*-nitroanilide) according to the previous methodology [42]. The tested samples' concentration was 1 to 10  $\mu\text{M}$  and the total incubation time in fMLF/CB-induced cells was 15 min. Genistein was used as the positive control. Cytotoxicity test was performed based on the release of LDH stored in the cytoplasm out of the cells [43]. Briefly, preheated (37  $^{\circ}\text{C}$ , 5 min, 1 mM  $\text{CaCl}_2$ ) human neutrophils ( $6 \times 10^5$  cells  $\cdot\text{mL}^{-1}$ ) were incubated with test compounds for 15 min. Total LDH release control was represented as completely lysed cells by 0.1% of Triton X-100 solution incubated with cells for 30 min. The cells were centrifuged at 4  $^{\circ}\text{C}$  for  $200 \times g$  for 8 min, and LDH reagent was added to supernatant and reacted at room temperature for 30 min in the dark. The absorbance was then measured at 492 nm, and the LDH release was calculated and compared to the total LDH release set as 100%.

### 3.6. Determination of Elastase Enzymatic Activity

The compounds were further tested for direct inhibition of elastase enzymatic activity [43]. The neutrophil suspension ( $6 \times 10^5$  cells  $\cdot\text{mL}^{-1}$ ) was preheated for 5 min in the presence of  $\text{CaCl}_2$  (1 mM) at 37  $^{\circ}\text{C}$ . Priming agent CB (1.5  $\mu\text{g mL}^{-1}$ ) was added for 2 min, followed by fMLF (0.1  $\mu\text{M}$ ) for 20 min to release the elastase from the cells. After centrifugation at 1000  $g$  for 5 min at 4  $^{\circ}\text{C}$ , the supernatant containing elastase was preheated at 37  $^{\circ}\text{C}$  for 5 min, and the test compounds were added. Then, 0.1 mM of substrate methoxysuccinyl-Ala-Ala-Pro-Val-*p*-nitroanilide was added for 10 min. The effect of the compounds on elastase enzymatic activity was quantified by measuring the absorbance at 405 nm.

### 3.7. Molecular Modeling Studies

Docking study was done using the procedure we reported and validated earlier [39]. Tested compounds were downloaded from Pubchem ([www.pubchem.ncbi.nlm.nih.gov](http://www.pubchem.ncbi.nlm.nih.gov), accessed on 10 May 2021) or built from the 2D structures. Ligands and proteins were prepared as reported earlier [44]. Docking analysis and image preparation were done using PyMol. The proposed binding mode of the isolated compounds with neutrophil elastase (NE) and SARS-CoV-2 main protease ( $\text{M}^{\text{Pro}}$ ) was studied using Autodock Vina and a method similar to what we reported earlier [39]. Here, crystal structures of NE (PDB ID:1H1B) and SARS-CoV-2  $\text{M}^{\text{Pro}}$  (PDB ID: 6LU7) were used. Prepared and co-crystallized ligands were docked in a grid box in the active site ( $25 \times 25 \times 25 \text{ \AA}^3$ , centered on co-crystallized ligand) using exhaustiveness of 16. For each ligand, the top nine binding poses were ranked according to their binding affinities and the predicted binding interactions were analyzed. The pose with the best binding affinity and binding mode similar to co-crystallized ligand was reported.

### 3.8. Coronavirus 229E Assay

The protective effects of the samples against human coronavirus 229E (HCoV-229) were determined similarly to the previously described method [45]. Huh7 cells (human liver carcinoma cell line) were infected with 9TCID50 (median tissue culture infectious dose) of each coronavirus 229E in the presence or absence of the compounds or vehicle. After incubation at 33  $^{\circ}\text{C}$  for 6 days, the surviving cells were then stained with MTT (3-[4,5-

dimethylthiazol-2-yl]-2,5-diphenyl tetrazolium bromide). The percentage of surviving cells was then calculated.

#### 4. Conclusions

Two butenolides, butyrolactons I (1) and III (2), along with one meroterpenoid, terretinin (3), and a prenylated hydroxybenzaldehyde derivative (4) were isolated from a marine-derived fungus *Aspergillus terreus*. Interestingly, butyrolactone I (1) revealed significant in vitro antiallergic, anti-inflammatory, and antielastase activity. These results were supported by molecular docking studies that also exhibited a possible potential role of 1 for inhibiting SARS-CoV-2 main protease, an essential enzyme for producing the viral functional proteins. These results shed more light on butyrolactone I (1) and other butenolide derivatives as potential candidates for developing lead compounds that may pave the way for producing new pharmaceuticals against SARS-CoV-2 and/or its pathological effects, in particular, ARDS, granting additional time for the immune system to fight for the patient's life.

**Supplementary Materials:** The following are available online, Figure S1: Human coronavirus 229E (HCoV-229E) protective activity, Table S1: <sup>1</sup>H and <sup>13</sup>C NMR Data of butyrolactone I (1), Table S2: <sup>1</sup>H and <sup>13</sup>C NMR Data of butyrolactone III (2), Table S3: <sup>1</sup>H and <sup>13</sup>C NMR Data of terretinin (3), Table S4: <sup>1</sup>H and <sup>13</sup>C NMR Data of 4-hydroxy-3-(3-methylbut-2-enyl)benzaldehyde (4).

**Author Contributions:** S.S.E., W.L. and B.K.: conceptualization, writing, reviewing and editing the manuscript; I.S.U., S.S.E. and B.K.: methodology, purification and isolation of pure metabolites; I.S.U., S.S.E. and B.K.: NMR analysis and data curation; A.A. and B.S.A.: molecular modeling; M.K. and B.-H.C.: antiallergy assay; Y.-H.W. and T.-L.H.: anti-inflammatory assay; J.-T.H.: coronavirus 229E assay. All authors have read and agreed to the published version of the manuscript.

**Funding:** This research was funded by TÜBİTAK-BMBF Project No: 114S916. This research was supported by the grants from the Ministry of Science and Technology (MOST 106-2320-B-255-003-MY3 and MOST 108-2320-B-255-003-MY3, MOST 109-2327-B-255-001, and MOST 109-2327-B-182-002), Chang Gung Memorial Hospital (CMRPF1G0241~3, CMRPF1J0051~3, and BMRP450), and Chang Gung University (104-6576A3), Taiwan. The funders had no role in the study design, data collection and analysis, decision to publish, or preparation of the manuscript.

**Institutional Review Board Statement:** Not applicable.

**Informed Consent Statement:** Not applicable.

**Data Availability Statement:** Data are available upon request from authors.

**Acknowledgments:** S.S.E. acknowledges The Scientific and Technological Research Council of Turkey (TÜBİTAK) for a financially supported visiting scientist fellowship.

**Conflicts of Interest:** The authors declare no conflict of interest.

**Sample Availability:** Samples of compounds (1 and 2) are available from the authors upon request.

#### References

1. Rothan, H.A.; Byrareddy, S.N. The epidemiology and pathogenesis of coronavirus disease (COVID-19) outbreak. *J. Autoimmun.* **2020**, *108*, 102433. [CrossRef]
2. da Silva, P.G.; Mesquita, J.R.; Nascimento, M.D.J.; Ferreira, V.A.M. Viral, host and environmental factors that favour zoonotic spillover of coronaviruses: An opinionated review, focusing on SARS-CoV, MERS-CoV and SARS-CoV-2. *Sci. Total Environ.* **2021**, *750*, 141483. [CrossRef]
3. Pfizer-BioNtech COVID-19 Vaccine. Available online: <https://www.fda.gov/emergency-preparedness-and-response/coronavirus-disease-2019-covid-19/pfizer-biontech-covid-19-vaccine> (accessed on 4 January 2021).
4. COVID-19: Oxford-AstraZeneca Vaccine Approved for Use in UK. Available online: <https://www.bbc.com/news/health-55280671> (accessed on 4 January 2021).
5. Risk Assessment: Risk related to Spread of New SARS-CoV-2 Variants of Concern in the EU/EEA. Available online: <https://www.ecdc.europa.eu/en/publications-data/covid-19-risk-assessment-spread-new-sars-cov-2-variants-eueea> (accessed on 4 January 2021).

6. Henriksen, P.A. The potential of neutrophil elastase inhibitors as anti-inflammatory therapies. *Curr. Opin. Hematol.* **2014**, *21*, 23–28. [[CrossRef](#)]
7. Hoenderdos, K.; Condliffe, A. The neutrophil in chronic obstructive pulmonary disease. *Am. J. Respir. Cell. Mol. Biol.* **2013**, *48*, 531–539. [[CrossRef](#)]
8. Moraes, T.J.; Chow, C.W.; Downey, G.P. Proteases and lung injury. *Crit. Care Med.* **2003**, *31*, S189–S194. [[CrossRef](#)]
9. Chiang, C.-C.; Korinek, M.; Cheng, W.-J.; Hwang, T.-L. Targeting neutrophils to treat acute respiratory distress syndrome in coronavirus disease. *Front. Pharmacol.* **2020**, *11*, 572009. [[CrossRef](#)]
10. Zhang, Y.L.; Zhang, J.; Jiang, N.; Lu, Y.H.; Wang, L.; Xu, S.H.; Wang, W.; Zhang, G.F.; Xu, Q.; Ge, H.M.; et al. Immunosuppressive polyketides from mantis-associated *Daldinia eschscholzii*. *J. Am. Chem. Soc.* **2011**, *133*, 5931–5940. [[CrossRef](#)]
11. Ebada, S.S.; El-Neketi, M.; Ebrahim, W.; Mándi, A.; Kurtán, T.; Kalscheuer, R.; Müller, W.E.G.; Proksch, P. Cytotoxic secondary metabolites from the endophytic fungus *Aspergillus versicolor* KU258497. *Phytochem. Lett.* **2018**, *24*, 88–93. [[CrossRef](#)]
12. Wang, Y.; Zheng, J.K.; Liu, P.P.; Wang, W.; Zhu, W.M. Three new compounds from *Aspergillus terreus* PT06-2 grown in a high salt medium. *Mar. Drugs* **2011**, *9*, 1368–1378. [[CrossRef](#)]
13. Liao, W.Y.; Shen, C.N.; Lin, L.H.; Yang, Y.L.; Han, H.Y.; Chen, J.W.; Kuo, S.C.; Wu, S.H.; Liaw, C.C. Asperjinone, a Nor-Neolignan, and terrein, a suppressor of ABCG2-expressing breast cancer cells, from thermophilic *Aspergillus terreus*. *J. Nat. Prod.* **2012**, *75*, 630–635. [[CrossRef](#)]
14. Deng, C.M.; Huang, C.H.; Wu, Q.L.; Pang, J.Y.; Lin, Y.C. A new sesquiterpene from the mangrove endophytic fungus *Aspergillus terreus* (No. GX7-3B). *Nat. Prod. Res.* **2013**, *27*, 1882–1887. [[CrossRef](#)]
15. Wijeratne, E.M.K.; Turbyville, T.J.; Zhang, Z.G.; Bigelow, D.; Pierson, L.S.; VanEtten, H.D.; Whitesell, L.; Canfield, L.M.; Gunatilaka, A.A.L. Cytotoxic constituents of *Aspergillus terreus* from the rhizosphere of *Opuntia versicolor* of the Sonoran Desert. *J. Nat. Prod.* **2003**, *66*, 1567–1573. [[CrossRef](#)] [[PubMed](#)]
16. Ebada, S.S.; Ebrahim, W. A new antibacterial quinolone derivative from the endophytic fungus *Aspergillus versicolor* strain Eich.5.2.2. *S. Afr. J. Bot.* **2020**, *134*, 151–155. [[CrossRef](#)]
17. Zhou, M.; Miao, M.M.; Du, G.; Li, X.N.; Shang, S.Z.; Zhao, W.; Liu, Z.H.; Yang, G.Y.; Che, C.T.; Hu, Q.F.; et al. Aspergillines A-E, highly oxygenated hexacyclic indole-tetrahydrofuran-tetramic acid derivatives from *Aspergillus versicolor*. *Org. Lett.* **2014**, *16*, 5016–5019. [[CrossRef](#)]
18. Gao, H.Q.; Zhou, L.N.; Cai, S.X.; Zhang, G.J.; Zhu, T.J.; Gu, Q.Q.; Li, D.H. Diorcinols B-E, new prenylated diphenyl ethers from the marine-derived fungus *Aspergillus versicolor* ZLN-60. *J. Antibiot.* **2013**, *66*, 539–542. [[CrossRef](#)] [[PubMed](#)]
19. Ji, N.Y.; Liu, X.H.; Miao, F.P.; Qiao, M.F. Aspeverin, a new alkaloid from an algicolous strain of *Aspergillus versicolor*. *Org. Lett.* **2013**, *15*, 2327–2329. [[CrossRef](#)]
20. Wang, W.; Kim, H.; Nam, S.J.; Rho, B.J.; Kang, H. Antibacterial butenolides from the Korean tunicate *Pseudodistoma antinboja*. *J. Nat. Prod.* **2012**, *75*, 2049–2054. [[CrossRef](#)]
21. Bai, Z.Q.; Lin, X.P.; Wang, Y.Z.; Wang, J.F.; Zhou, X.F.; Yang, B.; Liu, J.; Yang, X.W.; Wang, Y.; Liu, Y.H. New phenyl derivatives from endophytic fungus *Aspergillus flavipes* AIL8 derived of mangrove plant *Acanthus ilicifolius*. *Fitoterapia* **2014**, *95*, 194–202. [[CrossRef](#)]
22. Qin, J.J.; Zhu, J.X.; Zeng, Q.; Cheng, X.R.; Zhu, Y.; Zhang, S.D.; Shan, L.; Jin, H.Z.; Zhang, W.D. Pseudoguaianolides and guaianolides from *Inula hupehensis* as potential anti-inflammatory agents. *J. Nat. Prod.* **2011**, *74*, 1881–1887. [[CrossRef](#)]
23. Dewi, R.T.; Tachibana, S.; Darmawan, A. Effect on  $\alpha$ -glucosidase inhibition and antioxidant activities of butyrolactone derivatives from *Aspergillus terreus* MC751. *Med. Chem. Res.* **2014**, *23*, 454–460. [[CrossRef](#)]
24. Lin, X.; Li, K.; Yang, L.; Peng, X.; Fang, W.; Tian, X.; Liu, Y.; Zhou, X. Dereplication and targeted isolation of bioactive Sulphur compounds from bacteria isolated from a hydrothermal field. *Nat. Prod. Res.* **2019**, *33*, 494–499. [[CrossRef](#)] [[PubMed](#)]
25. Kiriya, N.; Nitta, K.; Sakaguchi, Y.; Taguchi, Y.; Yamamoto, Y. Studies on the metabolic products of *Aspergillus terreus*. III. Metabolites of the strain IFO 8835. *Chem. Pharm. Bull.* **1977**, *25*, 2593–2601. [[CrossRef](#)]
26. Rao, K.V.; Sadhukhan, A.K.; Veerender, M.; Ravikumar, V.; Mohan, E.V.S.; Dhanvantri, S.D.; Sitaramkumar, M.; Babu, J.M.; Vyas, K.; Reddy, G.O. Butyrolactones from *Aspergillus terreus*. *Chem. Pharm. Bull.* **2000**, *48*, 559–562. [[CrossRef](#)]
27. Niu, X.; Dahse, H.-M.; Menzel, K.-D.; Lozach, O.; Walther, G.; Meijer, L.; Grabley, S.; Sattler, I. Butyrolactone I derivatives from *Aspergillus terreus* carrying an unusual sulfate moiety. *J. Nat. Prod.* **2008**, *71*, 689–692. [[CrossRef](#)]
28. Nitta, K.; Fujita, N.; Yoshimura, T.; Arai, K.; Yamamoto, Y. Metabolic products of *Aspergillus terreus*. IX. Biosynthesis of butyrolactone derivatives isolated from strains IFO 8835 and 4100. *Chem. Pharm. Bull.* **1983**, *31*, 1528–1533. [[CrossRef](#)]
29. Chen, M.; Wang, K.-L.; Liu, M.; She, Z.-G.; Wang, C.-Y. Bioactive steroid derivatives and butyrolactone derivatives from a gorgonian-derived fungus *Aspergillus* sp. fungus. *Chem. Biodivers.* **2015**, *12*, 1398–1406. [[CrossRef](#)]
30. Springer, J.P.; Dorner, J.W.; Cole, R.J.; Cox, R.H. Terretonin, a toxic compound from *Aspergillus terreus*. *J. Org. Chem.* **1979**, *44*, 4852–4854. [[CrossRef](#)]
31. Li, G.-Y.; Li, B.-G.; Yang, T.; Yin, J.-H.; Qi, H.-Y.; Liu, G.-Y.; Zhang, G.-L. Sesterterpenoids, terretonins A-D, and an alkaloid, asterrelenin, from *Aspergillus terreus*. *J. Nat. Prod.* **2006**, *68*, 1243–1246. [[CrossRef](#)]
32. Hansson, D.; Menkis, A.; Olson, A.; Stenlid, J.; Broberg, A.; Karlsson, M. Biosynthesis of fomannoxin in the root rotting pathogen. *Heterobasidion occidentale*. *Phytochemistry* **2012**, *84*, 31–39. [[CrossRef](#)]
33. Vu, M.; Herfindal, L.; Juvik, O.J.; Vedeler, A.; Haavik, S. Toxic aromatic compounds from fruits of *Nartheceum ossifragum* L. *Phytochemistry* **2016**, *132*, 76–85. [[CrossRef](#)]

34. Liu, Q.-M.; Xie, C.-L.; Gao, Y.-Y.; Liu, B.; Lin, W.-X.; Liu, H.; Cao, M.-J.; Su, W.-J.; Yang, X.-W.; Liu, G.-M. Deep-sea-derived butyrolactone I suppresses ovalbumin-induced anaphylaxis by regulating mast cell function in a murine model. *J. Agric. Food Chem.* **2018**, *66*, 5581–5592. [[CrossRef](#)] [[PubMed](#)]
35. Jin, Z.; Du, X.; Xu, Y.; Deng, Y.; Liu, M.; Zhan, Y.; Zhang, B.; Li, X.; Zhang, L.; Peng, C.; et al. Structure of M<sup>Pro</sup> from SARS-CoV-2 and discovery of its inhibitors. *Nature* **2020**, *582*, 289–293. [[CrossRef](#)]
36. Sacco, M.D.; Ma, C.; Lagarias, P.; Gao, A.; Townsend, J.A.; Meng, X.; Dube, P.; Zhang, X.; Hu, Y.; Kitamura, N.; et al. Structure and inhibition of the SARS-CoV-2 main protease reveal strategy for developing dual inhibitors against M<sup>Pro</sup> and cathepsin L. *Sci. Adv.* **2020**, *6*, eabe0751. [[CrossRef](#)]
37. Zahran, E.M.; Albohy, A.; Khalil, A.; Ibrahim, A.H.; Ahmed, H.A.; El-hossary, E.M.; Bringmann, G.; Abdelmohsen, U.R. Bioactivity potential of marine natural products from scleractinia-associated microbes and in silico anti-SARS-CoV-2 evaluation. *Mar. Drugs* **2020**, *18*, 645. [[CrossRef](#)] [[PubMed](#)]
38. Said, M.A.; Albohy, A.; Abdelrahman, M.A.; Ibrahim, H.S. Importance of glutamine 189 flexibility in SARS-CoV-2 main protease: Lesson learned from in silico virtual screening of ChEMBL database and molecular dynamics. *Eur. J. Pharm. Sci.* **2021**, *160*, 105744. [[CrossRef](#)] [[PubMed](#)]
39. Ebada, S.S.; Al-Jawabri, N.A.; Youssef, F.S.; El-Kashef, D.H.; Knedel, T.-O.; Albohy, A.; Korinek, M.; Hwang, T.-L.; Chen, B.-H.; Lin, G.-H.; et al. Anti-inflammatory, antiallergic and COVID-19 protease inhibitory activities of phytochemicals from the Jordanian hawksbeard: Identification, structure-activity relationships, molecular modeling and impact on its folk medicinal uses. *RSC Adv.* **2020**, *10*, 38128–38141. [[CrossRef](#)]
40. Macdonald, S.J.F.; Dowle, M.D.; Harrison, L.A.; Clarke, G.D.F.; Inglis, G.G.A.; Johnson, M.R.; Shah, P.; Smith, R.A.; Amour, A.; Fleetwood, G.; et al. Discovery of further pyrrolidine *trans*-lactams as inhibitors of human neutrophil elastase (HNE) with potential as development candidates and the crystal structure of HNE complexed with an inhibitor (GW475151). *J. Med. Chem.* **2002**, *45*, 3878–3890. [[CrossRef](#)] [[PubMed](#)]
41. Korinek, M.; Wagh, V.D.; Lo, I.-W.; Hsu, Y.-M.; Hsu, H.-Y.; Hwang, T.-L.; Wu, Y.-C.; Cheng, Y.-B.; Chen, B.-H.; Chang, F.-R. Antiallergic phorbol ester from the seeds of *Aquilaria malaccensis*. *Int. J. Mol. Med.* **2016**, *17*, 398. [[CrossRef](#)]
42. Korinek, M.; Tsai, Y.H.; El-Shazly, M.; Lai, K.H.; Backlund, A.; Wu, S.F.; Lai, W.C.; Wu, T.Y.; Chen, S.L.; Wu, Y.C.; et al. Antiallergic hydroxy fatty acids from *Typhonium blumei* explored through ChemGPS-NP. *Front. Pharmacol.* **2017**, *8*, 356. [[CrossRef](#)] [[PubMed](#)]
43. Tsai, Y.F.; Yu, H.P.; Chang, W.Y.; Liu, F.C.; Huang, Z.C.; Hwang, T.L. Sirtinol inhibits neutrophil elastase activity and attenuates lipopolysaccharide-mediated acute lung injury in mice. *Sci. Rep.* **2015**, *5*, 8347. [[CrossRef](#)]
44. Ebada, S.S.; Al-Jawabri, N.A.; Youssef, F.S.; Albohy, A.; Aldalaien, S.M.; Disi, A.M.; Proksch, P. In vivo antiulcer activity, phytochemical exploration, and molecular modelling of the polyphenolic-rich fraction of *Crepis sancta* extract. *Inflammopharmacology* **2020**, *28*, 321–331. [[CrossRef](#)]
45. Hsieh, C.-F.; Jheng, J.-R.; Lin, G.-H.; Chen, Y.-L.; Ho, J.Y.; Liu, C.-J.; Hsu, K.-Y.; Chen, Y.-S.; Chan, Y.F.; Yu, H.-M.; et al. Rosmarinic acid exhibits broad anti-enterovirus A71 activity by inhibiting the interaction between the five-fold axis of capsid VP1 and cognate sulfated receptors. *Emerg. Microbes Infect.* **2020**, *9*, 1194–1205. [[CrossRef](#)]